Simulating the spatiotemporal variations in aboveground biomass in Inner Mongolian grasslands under environmental changes

Guocheng Wang[1], Zhongkui Luo[2], Yao Huang[3], Wenjuan Sun[3], Yurong Wei[4], Xi Deng[5], Jinhuan Zhu[6], Tingting Li[1], Wen Zhang[1]

[1]LAPC, Institute of Atmospheric Physics, Chinese Academy of Sciences, Beijing, 100029, China.
[2]College of Environmental and Resource Sciences, Zhejiang University, Hangzhou 310058, Zhejiang, China.
[3]State Key Laboratory of Vegetation and Environmental Change, Institute of Botany, Chinese Academy of Sciences, Beijing 100093, China.
[4]Inner Mongolia Ecology and Agrometeorology Centre, Hohhot, Inner Mongolia 100051, China.
[5]School of Atmospheric Sciences and Guangdong Province Key Laboratory for Climate Change and Natural Disaster Studies, Sun Yat-sen University, Zhuhai 519000, China
[6]LAOR, Institute of Atmospheric Physics, Chinese Academy of Sciences, Beijing, 100029, China.

Correspondence to: Guocheng Wang (wanggc@mail.iap.ac.cn)

Abstract. Grassland aboveground biomass (AGB) is a critical component of the global carbon cycle and reflects ecosystem productivity. Although it is widely acknowledged that dynamics of grassland biomass are significantly regulated by climate change, *in situ* evidence at large spatiotemporal scales is limited. Here, we combine biomass measurements from six long-term (> 30 years) experiments and data in existing literatures to explore the spatiotemporal changes in AGB in Inner Mongolian temperate grasslands. We show that, on average, annual AGB over the past four decades is 2,561 kg ha^{-1}, 1,496 kg ha^{-1} and 835 kg ha^{-1}, respectively, in meadow steppe, typical steppe and desert steppe in Inner Mongolia. The spatiotemporal changes of AGB are regulated by interactions of climatic attributes, edaphic properties, grazing intensity and grassland type. Using a machine learning-based approach, we map annual AGB (from 1981 to 2100) across the Inner Mongolian grassland at the spatial resolution of 1 km. We find that on the regional scale, meadow steppe has the highest annual AGB, followed by typical and desert steppe. Climate change characterized mainly by warming in the future could lead to a general decrease in grassland AGB. On average, compared with the historical AGB (i.e., average of 1981-2019), the AGB at the end of this century (i.e., average of 2080-2100) would decrease by 14% under RCP4.5 and 28% under RCP8.5, respectively. If the carbon dioxide (CO_2) enrichment effect on AGB is considered, however, the decreases in AGB can be reversed due to increased atmospheric CO_2 concentrations under RCP4.5 and RCP8.5 in the future. The projected changes in AGB show large spatial and temporal disparities across different grassland types and future climate change scenarios. Our results demonstrate the accuracy of predictions in AGB using a machine learning-based approach driven by several readily obtainable environmental variables; and provide new data at large scale and fine resolution extrapolated from field measurements.

1 Introduction

Grassland occupies ~40% of the world land and is an essential component of global terrestrial ecosystems (Hufkens et al., 2016). Grassland provides plenty of ecosystem services such as suppling food to livestock therefore meat and milk to humans

(Sattari et al., 2016) and accumulating carbon from atmosphere thus mitigating global warming (O'Mara, 2012). All of these functions are more or less directly dependent on grassland biomass, which has been recognized significantly influenced by environmental changes and anthropogenic activities (Hovenden et al., 2019). Thus, quantifying the dynamics of grassland biomass and revealing underlying mechanisms, particularly at large extents of space and time, are of fundamental importance (Andresen et al., 2018).

Dynamics of grassland biomass are driven by complex interactions among a series of environmental attributes, among which climate is one of the most predominant drivers (De Boeck et al., 2008;Wang et al., 2020a). The magnitudes and directions of climate change effects on AGB can vary across different local environments as well. For example, climate warming can either avail to biomass accumulation through reducing constraints of low temperature on plant growth (Gonsamo et al., 2018;Park et al., 2019) or go against biomass growth by aggravating the negative effects of water limitation on plant growth (Fan et al., 2009;Hu et al., 2007). This indicate the co-regulating effects of other local environmental attributes on plant biomass formations. In addition, in most existing studies, the mean annual climate attributes (e.g., temperature and precipitation) have widely been treated as the potential drivers on spatiotemporal changes in grassland biomass (Fan et al., 2009;Ma et al., 2008). However, growing evidences have demonstrated the importance of seasonality and intra-annual variability of climate, rather than the mean annual climate attributes, in regulating the grassland biomass dynamics (Godde et al., 2020;Grant et al., 2014). These effects of seasonality and intra-annual variability in climates have seldom been considered in studies focusing on large spatial extents, e.g., Inner Mongolia, where China's largest temperate grassland locates in. Moreover, existing studies have seldom considered the possible co-regulating effects of soil properties (Bhandari and Zhang, 2019;Jia et al., 2011), grassland types and grazing intensity (Eldridge and Delgado-Baquerizo, 2017) on AGB, which might lead to large uncertainties and biases in these estimations. Consequently, we need to explicitly take into account the seasonality of climate, soil, grassland type and grazing intensity in assessing the spatiotemporal variations in AGB rather than only considering the mean annual climate attributes such as temperature and precipitation.

It is noted that Inner Mongolian grassland accounts for more than half of China's northern temperate grassland area (Department of Animal Husbandry and Veterinary, 1996) and has the nation's largest grassland biomass carbon stock (Piao et al., 2004). The annual productivity of Inner Mongolian grassland, however, tends to vary in response to climate change (Bai et al., 2008). Since the start of 1980s, warming took place in many parts of Inner Mongolia (Wang et al., 2019). Under this warming, the spatiotemporal changes in grassland AGB, however, is still unclear. Although efforts have been taken to quantify AGB variations at the regional scale, these quantifications using mainly remote-sensing approaches generally show large disparities (Guo et al., 2016;Long et al., 2010;Ma et al., 2010a). Evidences from the datasets independent of remote sensing products may help to disentangle the mysterious spatiotemporal dynamics of AGB at the regional scale. In addition, the climate in the future is projected to experience substantial changes (IPCC, 2007) and thus significantly affect grassland AGB dynamics while little is known about the consequences of the likely future climate change on AGB across time and space. Furthermore,

it has been reported that carbon dioxide (CO_2) enrichment may increase plant productivity through enhancing photosynthetic rates and reducing stomatal conductance thereby increasing water use efficiency (Fay et al., 2012;Pastore et al., 2019). In general, the CO_2 enrichment induced increases in AGB might mitigate or even reverse the warming induced decreases in grassland AGB (Lee et al., 2010), which however has been seldom been assessed in Inner Mongolian grasslands at the regional scale. It is also worth noticed that the actual effects of CO_2 enrichment on AGB depend on local environmental factors such as water availability (Brookshire and Weaver, 2015) and soil texture (Polley et al., 2019), which can substantially affect the actual directions and magnitudes in AGB dynamics.

In this study, we collate to date the most comprehensive dataset of *in situ* measurements on plant biomass and climatic records in Inner Mongolian grassland from six long-term (more than 30 year) experiments and those data in the region from existing literatures. We calibrate and validate a machine learning-based model for predicting the aboveground biomass in the study region, by treating tens of environmental covariates (climates, soils, grazing intensity, and grassland type) as predicting variables. Then, we map the annual aboveground biomass at a spatial resolution of 1 km in Inner Mongolian grassland over the periods of 1981-2019 (using historical climatic dataset) and 2020-2100 [using climate projections driven by two representative concentration pathways (e.g., RCP4.5 and RCP8.5)]. In addition to predict the future dynamics of AGB driven by climate change characterized mainly by warming, we also aim to quantify the possible effect of CO_2 enrichment on AGB.

2 Materials and Methods

2.1 Study region and datasets of grassland aboveground biomass

The study region (i.e., Inner Mongolian grasslands) is characterized mainly by a temperate climate (Zhang et al., 2020) and thus is also called Inner Mongolian temperate grassland. The grasslands in the study region can be generally classified into three categories, i.e., meadow steppe, typical steppe and desert steppe (National Research Council, 1992). In brief, meadow steppe is distributed mainly in the eastern steppe zones, typical steppe locates mostly in the central Inner Mongolia, and desert steppe is found mainly to the west of the typical steppe (Fig. 1). In this study, we acquired two datasets of *in situ* aboveground biomass (AGB) in Inner Mongolian grassland. First, we obtained the AGB at six long-term (i.e., more than 30 years) experimental sites across the study region (Fig. 1a, Data S1). These six sites were established by Inner Mongolia Meteorological Bureau of China at early 1980s, measurements of AGB at each site has been carried out year by year since then. At each site, four fenced plots (i.e., four replicates) were set up to collect plant biomass data during plant growing seasons (e.g., from May to September). For each measurement replicate, the plants within a one square meter area were clipped and collected in a cloth bag. The samples were further air-dried to constant weights (weighted once every three days until the percent change in two consecutive weights are less than 2%). It is noted that plant growth rate could peak at different periods across time and space. Following Scurlock et al. (2002), we determined the annual plant biomass as the largest observed monthly biomass during a year (normally at the end of August at Ergun and at the end of September at other three sites). Apart

from these six long-term field experiments, we also retrieved a dataset regarding grassland AGB from Xu et al. (2018), who recently conducted a thorough literature synthesis and obtained a comprehensive dataset of plant biomass in the grasslands of northern China. For the dataset constructed by Xu et al. (2018), in this study, we use only the observations conducted in Inner Mongolian grassland and with investigation time and coordinates clearly reported (Fig. 1a). In general, the Inner Mongolian grassland AGB derived from these two datasets (i.e., long-term experiments and literature synthesis) are comparable (Fig. S1). In total, we obtained 511 individual measurements across 247 locations in Inner Mongolian temperate grasslands (Fig. 1a, Data S1).

2.2 Environmental covariates

Environmental covariates including climate, soil, grassland type and grazing intensity were retrieved for both AGB driver assessment and model fitting. For climatic covariates, we first obtained the daily climatic records of 120 climatic stations established in Inner Mongolia (Fig. 1b) from the National Meteorological Information Centre (NMIC) of China. The daily climatic attributes such as minimum, average and maximum temperature and precipitation were transformed into monthly time series data using the *daily2monthly* function in the R package *hydroTSM*. Based on these monthly data, we calculated 23 bioclimatic variables (Table 1) with an annual time step over the period of 1981-2019 by using the *biovars* function in the R package *dismo*. By doing so, we aim to comprehensively consider the possible effects of seasonality, intra- and inter-annual variability of climates (Fick and Hijmans, 2017). By further applying a interpolation algorithm (Thornton et al., 1997) to these 23 bioclimatic variables at the 120 stations, we created the raster layers of the climatic attributes with a spatial resolution of 1 km year by year. For the edaphic covariates, we directly extracted 10 raster soil layers representing key soil physical and chemical properties (Table 1) at a 1 km spatial resolution in the study region from ISRIC-WISE soil profile database (Batjes, 2016).

The grazing intensity in this study was represented by the quantity of three key animals (i.e., cattle, sheep and goats; Table 1) because they are the majority in Inner Mongolian grasslands (National Bureau of Statistics of China, 1981-2019). Here, we first derived the regional distribution data for cattle (Fig. S2 a), goat (Fig. S2 b) and sheep (Fig. S2 c) during 2010 in the study region from Gilbert et al. (2018). Then, we obtained the yearly total amount of each livestock in the study region (Fig. S2 d) from National Bureau of Statistics of China (1981-2019). By assuming a similar spatial distribution of livestock over time, we generated raster layers of each of the three animals year by year over the past four decades using the above-mentioned two datasets. In addition, a spatial layer of grassland type (i.e., meadow steppe, typical steppe and desert steppe; Fig. 1a and Table 1) at 1 km resolution was derived from the Vegetation Map of China (Zhang, 2007), the digital version of which is publicly obtainable (http://data.casearth.cn/sdo/detail/5c19a5680600cf2a3c557b6b).

2.3 Machine learning models to predict grassland biomass

To predict grassland aboveground biomass (AGB) across the region, we generated a suite of machine learning-based predictive models for AGB, treating edaphic, climatic, grassland type and grazing intensity (Table 1) as candidate predictors. Here, data from the 511 measurements (Fig. 1a and Data S1) were used to fit the models. For the spatial layers of soil properties and grassland type, which were assumed to be constant over time, we retrieved the associated covariates using the geographical coordinates of the 511 measurements. For those variables varying over time (e.g., climatic variables and grazing intensities), we extracted the associated attributes using both the locations and investigating year of the 511 measurements. In fitting the models, AGB is treated as a dependent variable and the environmental covariates (Table 1) are treated as independent variables. Before fitting the models, we converted the categorical variables (i.e., grassland type) to dummy variables. This is to avoid simply deducing the dependent variables in a certain category using the independent variables (e.g., climate variables) across other categories in building the machine learning models. Then, the function *findCorrelation* in R package *caret* was used to exclude the environmental covariates with high multicollinearities. Following Brownlee (2016), the remaining attributes were further adopted in model training (80% stratified samples) and validation (the remaining 20% stratified samples). We used a 10-fold cross-validation to train a suite of machine learning models using three algorithms [i.e., random forest (RF), Cubist and support vector machines (SVM)], which are implemented in the R package *caret*. The amount of variance in AGB explained by each model was assessed by the coefficient of determination (R^2). The root mean square error (RMSE, kg ha^{-1}) was also calculated ($RMSE = \sqrt{\sum_{i=1}^{n} \frac{(P_i - O_i)^2}{n}}$, where n is sample size, P_i and O_i are the i_{th} predicted and observed AGB, respectively) to compare the model simulations and observations. Apart from the three individual models, we also derived an ensemble model by adopting a principal component analysis (PCA) approach based on the predictions of the three algorithms. In brief, the smaller an individual model's RMSE is, the more the model's output contributes to final predictions.

2.4 Assessment of drivers on AGB

We used three approaches to explore the effects of environmental covariates on grassland AGB. First, the machine learning models themselves provide assessments of the relative importance (RI) of each independent variable in predicting the dependent variable (e.g., grassland AGB in this study). In general, the greater the RI of a variable is, the larger its influence on AGB is. Second, we adopted the Mantel test (Mantel, 1967) to assess the relationship between similarity of different grassland types and the similarity of environmental covariates using the R package *vegan*. Here, the standardized Mantel's r (ranges from 0 to 1) is used to represent the strength of this relationship (the higher the Mantel's r is, the stronger the correlation is) and the associated significance is indicated by the *P* value determined from 999 randomization (Legendre and Fortin, 1989). Third, we conducted a path analysis by using three latent variables, i.e., climate, soil and grazing, to explore their regulating effects on AGB. For each latent variable of climate and soil, the specific indicators were pre-identified using the above-mentioned R function *findCorrelation* to exclude the covariates with high multicollinearities. In constructing the inner model matrix of the path model, we hypothesized all the three latent variables have direct effects on AGB and climate may also

indirectly affect AGB through influencing soil properties. Here, we adopted the partial least squares (PLS) approach (Sanchez, 2013) and used the R package *plspm* to perform the path analysis. In interpreting the path analysis results, it is noted that the loadings of an indicator show the correlations between a latent variable and its indicators and all the indicators were standardized before the path analysis was performed.

2.5 Regional mapping and uncertainty analysis

Using the fitted machine learning-based ensemble model, we mapped AGB in Inner Mongolian grassland (at a spatial resolution of 1 km) on an annual time step in the history and future. In mapping the historical AGB (i.e., during 1981-2019), the model is run using environmental covariates extracted from the regional data layers (see *Environmental covariates*). Prediction uncertainty was quantified using a Monte Carlo analysis to develop the probability density functions (PDF) for each edaphic, climatic and livestock variable within the ranges of mean ±10%. The ensemble machine learning model was then run for 200 times in each grid with each of independent variables assigned from the PDF. The average and coefficient variation (CV, calculated as the standard deviation divided by the average) were then determined in each grid using the 200 model outputs to represent the predicted AGB and the associated uncertainty, respectively.

For predictions of AGB in the future (i.e., 2020-2100), we include the climatic datasets projected by one typical CMIP5 global circulation model (GCM) to save computing resources. In this study, we use the projections output by CESM1-BGC, which was run by National Center for Atmospheric Research (NCAR). Here, we directly obtained the processed climatic products constructed by Karger et al. (2020), who recently generated a downscaled and bias-corrected temperature and precipitation datasets. Specifically, these future climatic datasets were driven by two scenarios of representative concentration pathways (RCP4.5 and RCP8.5) at monthly step in this century. According to the model projections, mean annual temperature (MAT) under both RCPs will continue to increase in the following decades (Fig. S3). The extent of climate warming is generally higher under RCP8.5 than that under RCP4.5 (Fig. S3). After obtaining the future climate datasets, we also use the *biovars* function in R environment (see *Environmental covariates*) to calculate the 23 interested bioclimatic attributes (Table 1) for both scenarios of RCPs year by year from 2020 to 2100. In projecting the future AGB dynamics using the ensemble machine learning model, we assume that the soil properties will not significantly change over time (i.e., the same soil inputs used in historical AGB predictions) and current grazing intensity will keep relatively stable (i.e., the average of the most recent five years). In addition, the uncertainty analysis for future AGB predictions were performed using the same approach as that adopted in mapping the historical AGB. Moreover, the CO_2 concentrations have been projected to increase under the two RCPs (i.e., RCP4.5 and RCP8.5) used in this study (Fig. S4 a), which can potentially either increase AGB through enhanced photosynthetic rates (Fay et al., 2012;Lee et al., 2010) or have limited influences because of other environmental constraints on plant growth (Brookshire and Weaver, 2015). In this study, we deduced future AGB dynamics with both including and not including the effect of CO_2 enrichment on grassland AGB. In including CO_2 enrichment effect, we used the relationship between CO_2 concentration and ANPP based on long-term experimental data derived from Polley et al. (2019). Specifically,

we assume a general linear response of AGB to increased CO_2 concentrations, i.e., an increase of 100 ppm in CO_2 leads to an increase of 850 kg ha^{-1} in grassland AGB (Fig. S4 b). This linearly positive effect of CO_2 on AGB is further applied to the machine learning models predicted future AGB (i.e., the AGB not including CO_2 enrichment effect). Here, for each RCP scenario, we used the annual CO_2 concentrations in the future (Fig. S4 a) and the average annual CO_2 concentration over 2014-2019 as a baseline to determine the increment in AGB at each year from 2020 to 2100. All statistical analyses and graphical productions in this study were performed in R v3.6.3 (R Development Core Team, 2020).

3 Results

The field observations indicate that, on average, aboveground biomass (AGB) in Inner Mongolian grassland is 1,700 kg ha^{-1} ranging from 220 kg ha^{-1} [2.5% confidence intervals (CI)] to 4,827 kg ha^{-1} (97.5% CI, Fig. 2). Across the three grassland types, meadow steppe has the highest AGB (2,561 Mg ha^{-1} ranging from 736 Mg ha^{-1} to 5,537 Mg ha^{-1}), followed by typical steppe (1,496 Mg ha^{-1} ranging from 213 Mg ha^{-1} to 4,418 Mg ha^{-1}), and desert steppe has the lowest AGB (835 Mg ha^{-1} ranging from 234 Mg ha^{-1} to 1,928 Mg ha^{-1}, Fig. 2).

The fitted three individual machine learning algorithms (i.e., RF, Cubist and SVM) can explain overall 32%-48% of the variance in observed AGB (Fig. 3a, b and c). The ensemble model of the three algorithms can better simulate the observations than any of those individual models (Fig. 3). On average, 52% of the variance in the observations can be explained by the ensemble model (Fig. 3d). Although the variable importance differed among the three algorithms, climatic and livestock variables seem to substantially affect the AGB dynamics (Fig. S5). After excluding the covariates with high multilinearities, the remaining 10 climatic attributes, 5 edaphic variables and three livestock predictors generally show small autocorrelations (Fig. 4a). Mantel test suggests that, compared to the edaphic and livestock attributes, the climatic variables are in general stronger correlators of AGB in the three grassland types (Fig. 4a). Furthermore, the path analysis suggests that AGB shows small correlations with climate (using the 10 climatic indicators identified by the analysis to exclude the environmental covariates with high multicollinearities, hereafter the same for soil) and soil (reflected by the five edaphic properties) while significantly and positively correlates with grazing (Fig. 4b). We also found that climate can indirectly affects AGB via its influence on soil (Fig. 4b). It should be noticed that the small average magnitude with large variabilities of the loadings for climate (Fig. 4b) suggests the corresponding indicators for climate may distinctly affect AGB dynamics. It should also be noted that the overall performance of the fitted path model (R^2=0.22, Fig. 4b) in explaining the variability of AGB is much smaller than those of the machine learning models (Fig. 3), which indicates that more complex and non-linear relationships of the environmental drivers may exist in regulating AGB dynamics.

The regional mapping results of grassland AGB during 1981-2019 show large spatial variations (Fig. 5a). On average, the regional AGB during the past four decades is 1,438 kg ha^{-1}, the corresponding lower and upper limits of the 95% CI is 479 kg ha^{-1}, and 2,284 kg ha^{-1}, respectively (Fig. 5a). Across grassland types, meadow steppe has the highest average AGB (2,194 Mg

ha^{-1} ranging from 1,153 Mg ha^{-1} to 2,631 Mg ha^{-1}), followed by typical steppe (1,552 Mg ha^{-1} ranging from 539 Mg ha^{-1} to 2,200 Mg ha^{-1}) and desert steppe (893 Mg ha^{-1} ranging from 405 Mg ha^{-1} to 1,341 Mg ha^{-1}, Fig. 5a). Spatially, the average coefficient of variation (CV) in the predictions is lowest in meadow steppe (10.5%), followed by desert steppe (14.6%) and typical steppe (21.8%, Fig. 5d). Over 1981-2019, the regional average AGB displayed a decreasing trend (Fig. 6a). Among the three grassland types, the historical changes in AGB (Fig. 6b, c and d) are in general consistent with that of the total Inner Mongolian grassland AGB (Fig. 6a). Moreover, the long-term field observations also show large inter-annual variabilities in the grassland biomass (Fig. 7) and can support our predicted temporal biomass dynamics at the regional scale (Fig. 6). For example, at four of the six sites, AGB showed a general decreasing trend (Fig. 7).

If the CO_2 enrichment effect on AGB is not considered, our predicting results show that future AGB in general decreases under both scenarios of RCPs (i.e., RCP4.5 and RCP8.5, Fig. 6 and Table 2). Compared with the historical AGB (i.e., average AGB during 1981-2019, hereafter the same), on average, AGB at the end of this century (i.e., average of 2080-2100, hereafter the same) would decrease by 14% under RCP4.5 (Fig. 5b) and 28% under RCP8.5, respectively (Table 2). The decreases in AGB under future climate change show large disparities across different grassland types and climate change scenarios. Compared with the historical average AGB, AGB at the end of this century under RCP4.5 is estimated to decrease by a smaller extent (i.e.,10%) in meadow steep than those in typical (16%) and desert steep (21%, Table 2). In general, AGB under RCP8.5 would reduce by larger extents compared with those under RCP4.5. Under RCP8.5, the average AGB at the end of this century is estimated to experience a 24% (in meadow steep), 30% (in typical steep) and 25% (in desert steep) reduction, compared with the averages over 1981-2019 (Table 2). The magnitudes and spatial patterns of CV in the simulations under both RCP4.5 (Fig. 5e) and RCP8.5 (Fig. 5f) are comparable with those during the period of 1981-2019 (Fig. 5d).

If the CO_2 enrichment effect on AGB is taken into account, the predicted losses in AGB can be reversed under both RCP scenarios (Fig. 8). By the end of this century, the regional average AGB is increased by 63% under RCP4.5 and 232% under RCP8.5, respectively, compared with the average AGB during 1981-2019 (Fig. 8a, Table 2). The increases in AGB under climate change including CO_2 enrichment effect also show large disparities in across grassland types. For example, under RCP4.5, the average AGB at the end of this century is estimated to increase by 40% in meadow steppe, 55% in typical steppe and 102% in desert steppe, respectively, compared with their counterparts during 1981-2019 (Fig. 8b, c and d, Table 2). The increases in AGB are much larger under RCP8.5 than those under RCP4.5. On average, under RCP8.5, the AGB at the end of this century is projected to enhance by 147%, 212% and 394% in meadow, typical and desert steppe, respectively, compared with those over 1981-2019 (Fig. 8b, c and d, Table 2).

4 Discussion

Our results, based on AGB observations derived from six long-term field experiments and literature synthesis, indicate the large spatial disparities in aboveground biomass across different grassland types (Fig. 2). This gradient spatial pattern in AGB,

i.e., largest in meadow steep followed by that in typical and desert steep, is comparable with Ma et al. (2008), who carried out a comprehensive field measurements and investigated 113 locations in Inner Mongolian temperate grassland during 2002-2005. On the regional scale, we mapped grassland AGB at high spatial and temporal resolutions, which shows that AGB generally decreases from north-eastern to south-western areas in the study region (Fig. 5a). Such a spatial pattern is also consistent with the maps generated from remote sensing derivations (Fig. S6). This demonstrates the accuracy of our machine learning model's predictions. It should be noted that existing mapping products of grassland AGB use mainly remote sensing approaches requiring inputs from satellite-based datasets (Guo et al., 2016;Jiao et al., 2019;Ma et al., 2010a). Our fitted machine learning model, however, uses only several readily obtainable environmental covariates (Fig. 4 and Table 1). Our results demonstrate the ability of machine learning approach to effectively extrapolate grassland AGB to much larger spatiotemporal extents (e.g., Fig. 5 and 6).

Our simulation results show that, under the climate warming over the past four decades (Fig. S3), the average AGB generally experienced a declining trend across all the three grassland types in Inner Mongolia (Fig. 6). This demonstrates the possible negative effect of temperature rising on AGB that has been widely reported (De Boeck et al., 2008;Wang et al., 2020a), particularly in the arid and semi-arid ecosystems (Ma et al., 2010b). This harmful influence of warming on AGB is explainable. For example, in a system restrained by water availability (e.g., temperate grassland), warming can not only inhibit plant photosynthesis (Xu and Zhou, 2005) but also enhance evaporation and further intensify water stress (De Boeck et al., 2006) thereby decreasing grassland biomass. Precipitation has generally been recognized to have positive effects on AGB in the temperate grassland (Hovenden et al., 2019;Ma et al., 2010a), which supports our findings in this study. For example, the simulated average AGB is relatively higher in the years with higher MAP (e.g., 1998 and 2012) than those in other years (Fig. 6a). The importance of precipitation on AGB can be more reflected by the spatial patterns of these two attributes, e.g., AGB is much lower in the more arid regions (Fig. 5a) where soils are suffering severer water deficiencies. Apart from climatic factors, our results also demonstrate the co-regulating effects of soil conditions and livestock on the dynamics of grassland AGB as indicated by the machine learning models (Fig. S5) and the path analysis model (Fig. 4b). This is consistent with several findings highlighting the importance of soil physical and chemical characteristics (Griffiths et al., 2012;Yang et al., 2009) and grazing intensity (Eldridge and Delgado-Baquerizo, 2017) in controlling grassland biomass changes. It should be noted that the major drivers of the simulated temporal changes in AGB (Fig. 6) can vary during different periods in this study due to data availability particularly for grazing intensity. Specifically, AGB dynamics over 1981-2019 is co-regulated by both changes in climates and grazing activities (Fig. S2, S3 and S5). In future scenario simulations (e.g., 2020-2100, Fig. 6), however, AGB variations are predominantly controlled by climates since a constant grazing intensity was adopted over time in future predictions. We admit that the actual grazing intensity can vary over time in the future depending on RCP scenarios, simply assuming a stable grazing intensity over time can lead to substantial biases in AGB estimations. We need novel approaches to derive the temporal variations in grazing intensity at high spatial resolutions under future RCP scenarios.

Our estimations indicate that AGB can be substantially increased under future CO_2 enrichment (Fig. 8). Here, several uncertainties and limitations should be noticed in interpreting this estimation. First, the gradient of CO_2 concentrations in (Polley et al., 2019), which is used to derive the effect of CO_2 enrichment on AGB, has a smaller range (i.e., 250 ppm to 500 ppm) than those under RCP8.5 (is projected to increase to around 900 ppm by the end of this century). Here, applying this relationship to larger extents may lead to substantial uncertainties in AGB. Second, the local soil (Fay et al., 2012) and climatic (Brookshire and Weaver, 2015) factors can modify the actual CO_2 enrichment effect on AGB, which may also result in large uncertainties in the estimations. For example, any stimulation in plant growth is constrained by the availability of other resources required by plant growth (Reyes-Fox et al., 2014) such as soil water availability (Brookshire and Weaver, 2015). Consequently, the magnitude of the increases in AGB induced by CO_2 enrichment estimated in this study, particularly under RCP8.5, can be largely overestimated due to the possible limitations of both nutrients and water required by plant growth (Wang et al., 2020b).

We also notice that our model predictions show larger interannual variations in AGB (Fig. 6a) than those in the estimations based on remote sensing approaches (Fig. S6). In fact, the remote sensing derived AGB has also been bias-corrected by the field measurements (Jiao et al., 2019). Consequently, this disparity could be related to the difference of observed AGB datasets used in different studies. Specifically, the measurements of biomass used to calibrate remote-sensing data [normalized difference vegetation index (NDVI)] in Jiao et al. (2019) were generally conducted during 2001-2015. Extrapolations of these observations from a short term (e.g., 2001-2015) to a much longer term (e.g., 1982-2015) might lead to underestimations in the long-term interannual variabilities. Our study, however, integrate the *in situ* observed data from six long-term (1982-2015) field experiments (Fig. 1a), which can potentially reduce the possible biases in model predictions. In addition, we find that the overall decrease in Inner Mongolian grassland biomass are contributed greater by the decline during the first three decades and the declining trend in AGB seems to be alleviated in the recent decade (Fig. 6). This could be related to the overall slowing climate warming over the recent decade (Fig. S3). In the future, a faster warming (e.g., RCP8.5) climate will lead to a larger reduction in grassland AGB (Fig. 5b and c). It is noteworthy that the accuracy of our predictions on future grassland AGB relies substantially on the robustness of future climate change projections simulated by the GCMs (e.g., CESM1-BGC). However, although CESM1-BGC (like all other CMIP5 models) can reasonably well simulate changes in temperature, it may not well predict precipitation, particularly for Eastern China where is strongly affected by large-scale atmospheric circulations (Huang et al., 2013). Consequently, it should be cautious in interpreting the likely decrease of AGB under future temperature rising (Fig. 6), because the large uncertainties in projected precipitation may lead to biased predictions in AGB.

5 Conclusions

Our results demonstrate that the aboveground biomass in Inner Mongolian grasslands shows large spatial and temporal variations during the past four decades, which is driven by a series of environmental covariates. Particularly, current climate

change characterized mainly by warming has negative effects on AGB across all types of grassland. The decreases of AGB induced by warming, however, can potentially be reversed by the CO_2 enrichment effect. In addition, our results demonstrate that adopting a machine learning model approach with only a few readily obtainable environmental predictors can accurately capture AGB dynamics, which enables extrapolations of AGB across larger spatiotemporal extents. Moreover, our study provides new data on annual AGB in the study region at fine spatial (1km) and temporal (yearly) resolutions for both historical (1981-2019) and future (2020-2100) periods under different climate change scenarios.

Data availability. The data that support the findings of this study (Data S1) are openly available at: 10.6084/m9.figshare.13108430.

Supplement. The supplement related to this article is available online at: XXX.

Author contributions. G. Wang and Y. Huang conceived this study. G. Wang conducted the data analysis with interpretations from Z. Luo and Y. Huang. G. Wang and Z. Luo prepared the article with contributions from all authors.

Competing interests. The authors declare that they have no conflict of interest.

Acknowledgements. The authors acknowledge the people who conducted the filed long-term experiments and collected the observed data.

Financial support. This study is financially supported by the National Natural Science Foundation of China (Grant No. 41775156 and 41590875) and the Strategic Priority Research Program of the Chinese Academy of Sciences (Grant No. XDA26010103).

References

Andresen, L. C., Yuan, N., Seibert, R., Moser, G., Kammann, C. I., Luterbacher, J., Erbs, M., and Müller, C.: Biomass responses in a temperate European grassland through 17 years of elevated CO_2, Global Change Biol, 24, 3875-3885, 2018.

Bai, Y., Han, X., Wu, J., Chen, Z., and Li, L.: Ecosystem stability and compensatory effects in the Inner Mongolia grassland, Nature, 431, 181-184, 2004.

Bai, Y., Wu, J., Xing, Q., Pan, Q., Huang, J., Yang, D., and Han, X.: Primary production and rain use efficiency across a precipitation gradient on the Mongolia plateau, Ecology, 89, 2140-2153, 2008.

Batjes, N. H.: Harmonized soil property values for broad-scale modelling (WISE30sec) with estimates of global soil carbon stocks, Geoderma, 269, 61-68, 10.1016/j.geoderma.2016.01.034, 2016.

Bhandari, J., and Zhang, Y.: Effect of altitude and soil properties on biomass and plant richness in the grasslands of Tibet, China, and Manang District, Nepal, Ecosphere, 10, e02915, 10.1002/ecs2.2915, 2019.

Brookshire, E. N. J., and Weaver, T.: Long-term decline in grassland productivity driven by increasing dryness, Nature Communications, 6, 10.1038/ncomms8148, 2015.

Brownlee, J.: Machine learning mastery with python, Machine Learning Mastery Pty Ltd, 100-120, 2016.

De Boeck, H. d., Lemmens, C., Zavalloni, C., Gielen, B., Malchair, S., Carnol, M., Merckx, R., Van den Berge, J., Ceulemans, R., and Nijs, I.: Biomass production in experimental grasslands of different species richness during three years of climate warming, Biogeosciences, 585-594, 2008.

De Boeck, H. J., Lemmens, C. M., Bossuyt, H., Malchair, S., Carnol, M., Merckx, R., Nijs, I., and Ceulemans, R.: How do climate warming and plant species richness affect water use in experimental grasslands?, Plant Soil, 288, 249-261, 2006.

Department of Animal Husbandry and Veterinary: Rangeland resources of China, China Science and Technology Press Beijing (in Chinese), 1996.

Eldridge, D. J., and Delgado-Baquerizo, M.: Continental-scale impacts of livestock grazing on ecosystem supporting and regulating services, Land Degradation & Development, 28, 1473-1481, 2017.

Fan, J., Wang, K., Harris, W., Zhong, H., Hu, Z., Han, B., Zhang, W., and Wang, J.: Allocation of vegetation biomass across a climate-related gradient in the grasslands of Inner Mongolia, J Arid Environ, 73, 521-528, 2009.

Fay, P. A., Jin, V. L., Way, D. A., Potter, K. N., Gill, R. A., Jackson, R. B., and Polley, H. W.: Soil-mediated effects of subambient to increased carbon dioxide on grassland productivity, Nature Climate Change, 2, 742-746, 10.1038/nclimate1573, 2012.

Fick, S. E., and Hijmans, R. J.: WorldClim 2: new 1-km spatial resolution climate surfaces for global land areas, Int J Climatol, 37, 4302-4315, 10.1002/joc.5086, 2017.

Gilbert, M., Nicolas, G., Cinardi, G., Van Boeckel, T. P., Vanwambeke, S. O., Wint, G. W., and Robinson, T. P.: Global distribution data for cattle, buffaloes, horses, sheep, goats, pigs, chickens and ducks in 2010, Scientific data, 5, 1-11, 2018.

Godde, C. M., Boone, R., Ash, A. J., Waha, K., Sloat, L., Thornton, P. K., and Herrero, M.: Global rangeland production systems and livelihoods at threat under climate change and variability, Environmental Research Letters, 15, 044021, 2020.

Gonsamo, A., Chen, J. M., and Ooi, Y. W.: Peak season plant activity shift towards spring is reflected by increasing carbon uptake by extratropical ecosystems, Global Change Biol, 24, 2117-2128, 2018.

Grant, K., Kreyling, J., Dienstbach, L. F., Beierkuhnlein, C., and Jentsch, A.: Water stress due to increased intra-annual precipitation variability reduced forage yield but raised forage quality of a temperate grassland, Agriculture, Ecosystems & Environment, 186, 11-22, 2014.

Griffiths, B. S., Spilles, A., and Bonkowski, M.: C:N:P stoichiometry and nutrient limitation of the soil microbial biomass in a grazed grassland site under experimental P limitation or excess, Ecological Processes, 1, 6, 10.1186/2192-1709-1-6, 2012.

Guo, L. H., Hao, C. Y., Wu, S. H., Zhao, D. S., and Gao, J. B.: Analysis of changes in net primary productivity and its susceptibility to climate change of Inner Mongolian grasslands using the CENTURY model, Geographical Research, 35, 271-284 (in Chinese with English abstract), 2016.

Hovenden, M. J., Leuzinger, S., Newton, P. C., Fletcher, A., Fatichi, S., Lüscher, A., Reich, P. B., Andresen, L. C., Beier, C., and Blumenthal, D. M.: Globally consistent influences of seasonal precipitation limit grassland biomass response to elevated CO 2, Nature plants, 5, 167-173, 2019.

Hu, Z., Fan, J., Zhong, H., and Yu, G.: Spatiotemporal dynamics of aboveground primary productivity along a precipitation gradient in Chinese temperate grassland, Sci China Ser D, 50, 754-764, 10.1007/s11430-007-0010-3, 2007.

Huang, D.-Q., Zhu, J., Zhang, Y.-C., and Huang, A.-N.: Uncertainties on the simulated summer precipitation over Eastern China from the CMIP5 models, Journal of Geophysical Research: Atmospheres, 118, 9035-9047, 10.1002/jgrd.50695, 2013.

Hufkens, K., Keenan, T. F., Flanagan, L. B., Scott, R. L., Bernacchi, C. J., Joo, E., Brunsell, N. A., Verfaillie, J., and Richardson, A. D.: Productivity of North American grasslands is increased under future climate scenarios despite rising aridity, Nature Climate Change, 6, 710-714, 2016.

IPCC: Climate change 2007: impacts, adaptation and vulnerability. Contribution of working group II to the fourth assessment report of the intergovernmental panel on climate change, Cambridge University Press, Cambridge, 2007.

Jia, X., Shao, M., Wei, X., Horton, R., and Li, X.: Estimating total net primary productivity of managed grasslands by a state-space modeling approach in a small catchment on the Loess Plateau, China, Geoderma, 160, 281-291, https://doi.org/10.1016/j.geoderma.2010.09.016, 2011.

Jiao, C. C., YU, G. R., Chen, Z., and He, N. P.: A dataset for aboveground biomass of the northern temperate and Tibetan Plateau alpine grasslands in China, based on field investigation and remote sensing inversion (1982–2015), China Scientific Data, 4, DOI: 10.11922/csdata.2018.0029.zh, 2019.

Karger, D. N., Schmatz, D. R., Dettling, G., and Zimmermann, N. E.: High-resolution monthly precipitation and temperature time series from 2006 to 2100, Scientific Data, 7, 248, 10.1038/s41597-020-00587-y, 2020.

Lee, M., Manning, P., Rist, J., Power, S. A., and Marsh, C.: A global comparison of grassland biomass responses to CO2 and nitrogen enrichment, Philosophical Transactions of the Royal Society B-Biological Sciences, 365, 2047-2056, 10.1098/rstb.2010.0028, 2010.

Legendre, P., and Fortin, M. J.: Spatial pattern and ecological analysis, Vegetatio, 80, 107-138, 1989.

Long, L. H., Li, X. B., Wang, H., Wei, D. D., and Zhang, C.: Net primary productivity (NPP) of grassland ecosystem and its relationship with climate in Inner Mongolia, Acta Ecologica Sinica, 30, 1367-1378 (in Chinese with English abstract), 2010.

Ma, W., Yang, Y., He, J., Zeng, H., and Fang, J.: Above-and belowground biomass in relation to environmental factors in temperate grasslands, Inner Mongolia, Science in China Series C: Life Sciences, 51, 263-270, 2008.

Ma, W., Fang, J., Yang, Y., and Mohammat, A.: Biomass carbon stocks and their changes in northern China's grasslands during 1982–2006, Science China Life Sciences, 53, 841-850, 2010a.

Ma, W., Liu, Z., Wang, Z., Wang, W., Liang, C., Tang, Y., He, J.-S., and Fang, J.: Climate change alters interannual variation of grassland aboveground productivity: evidence from a 22-year measurement series in the Inner Mongolian grassland, Journal of Plant Research, 123, 509-517, 10.1007/s10265-009-0302-0, 2010b.

Mantel, N.: The detection of disease clustering and a generalized regression approach, Cancer research, 27, 209-220, 1967.

National Research Council: Grasslands and Grassland Sciences in Northern China, The National Academies Press, Washington, DC, 230 pp., 1992.

O'Mara, F. P.: The role of grasslands in food security and climate change, Ann Bot-london, 110, 1263-1270, 2012.

Park, T., Chen, C., Macias-Fauria, M., Tømmervik, H., Choi, S., Winkler, A., Bhatt, U. S., Walker, D. A., Piao, S., and Brovkin, V.: Changes in timing of seasonal peak photosynthetic activity in northern ecosystems, Global Change Biol, 25, 2382-2395, 2019.

Pastore, M. A., Lee, T. D., Hobbie, S. E., and Reich, P. B.: Strong photosynthetic acclimation and enhanced water-use efficiency in grassland functional groups persist over 21 years of CO2 enrichment, independent of nitrogen supply, Global Change Biology, 25, 3031-3044, 10.1111/gcb.14714, 2019.

Piao, S., Fang, J., He, J., and Xiao, Y.: Spatial distribution of grassland biomass in China, Acta Phytoecologica Sinica, 28, 491-498(in Chinese with English Abstract), 2004.

Polley, H. W., Aspinwall, M. J., Collins, H. P., Gibson, A. E., Gill, R. A., Jackson, R. B., Jin, V. L., Khasanova, A. R., Reichmann, L. G., and Fay, P. A.: CO2 enrichment and soil type additively regulate grassland productivity, New Phytologist, 222, 183-192, 10.1111/nph.15562, 2019.

Reyes-Fox, M., Steltzer, H., Trlica, M. J., McMaster, G. S., Andales, A. A., LeCain, D. R., and Morgan, J. A.: Elevated CO2 further lengthens growing season under warming conditions, Nature, 510, 259-+, 10.1038/nature13207, 2014.

Sanchez, G.: PLS path modeling with R, Berkeley: Trowchez Editions, 383, 2013, 2013.

Sattari, S., Bouwman, A., Rodriguez, R. M., Beusen, A., and Van Ittersum, M.: Negative global phosphorus budgets challenge sustainable intensification of grasslands, Nature communications, 7, 1-12, 2016.

Scurlock, J. M., Johnson, K., and Olson, R. J.: Estimating net primary productivity from grassland biomass dynamics measurements, Global Change Biology, 8, 736-753, 2002.

Thornton, P. E., Running, S. W., and White, M. A.: Generating surfaces of daily meteorological variables over large regions of complex terrain, Journal of Hydrology, 190, 214-251, 1997.

Wang, G., Huang, Y., Wei, Y., Zhang, W., Li, T., and Zhang, Q.: Climate Warming Does Not Always Extend the Plant Growing Season in Inner Mongolian Grasslands: Evidence From a 30-Year In Situ Observations at Eight Experimental Sites, Journal of Geophysical Research: Biogeosciences, 124, 2364-2378, 10.1029/2019jg005137, 2019.

Wang, H., Liu, H., Cao, G., Ma, Z., Li, Y., Zhang, F., Zhao, X., Zhao, X., Jiang, L., and Sanders, N. J.: Alpine grassland plants grow earlier and faster but biomass remains unchanged over 35 years of climate change, Ecol Lett, 701-710, 10.1111/ele.13474, 2020a.

Wang, S., Zhang, Y., Ju, W., Chen, J. M., Ciais, P., Cescatti, A., Sardans, J., Janssens, I. A., Wu, M., Berry, J. A., Campbell, E., Fernández-Martínez, M., Alkama, R., Sitch, S., Friedlingstein, P., Smith, W. K., Yuan, W., He, W., Lombardozzi, D., Kautz, M., Zhu, D., Lienert, S., Kato, E., Poulter, B., Sanders, T. G. M., Krüger, I., Wang, R., Zeng, N., Tian, H., Vuichard, N., Jain, A. K., Wiltshire, A., Haverd, V., Goll, D. S., and Peñuelas, J.: Recent global decline of CO₂ fertilization effects on vegetation photosynthesis, Science, 370, 1295-1300, 10.1126/science.abb7772, 2020b.

Xu, L., Yu, G., He, N., Wang, Q., Gao, Y., Wen, D., Li, S., Niu, S., and Ge, J.: Carbon storage in China's terrestrial ecosystems: A synthesis, Scientific reports, 8, 1-13, 2018.

Xu, Z., and Zhou, G.: Effects of water stress and high nocturnal temperature on photosynthesis and nitrogen level of a perennial grass Leymus chinensis, Plant Soil, 269, 131-139, 2005.

Yang, Y., Fang, J., Pan, Y., and Ji, C.: Aboveground biomass in Tibetan grasslands, J Arid Environ, 73, 91-95, 2009.

Zhang, Q., Buyantuev, A., Fang, X., Han, P., Li, A., Li, F. Y., Liang, C., Liu, Q., Ma, Q., Niu, J., Shang, C., Yan, Y., and Zhang, J.: Ecology and sustainability of the Inner Mongolian Grassland: Looking back and moving forward, Landscape Ecology, 35, 2413-2432, 10.1007/s10980-020-01083-9, 2020.

Zhang, X.: Vegetation Map of China and Its Geographic Pattern: Illustration of the Vegetation Map of the People's Republic China (1: 10,000,000), Geological Press. 296–326., Beijing, 2007.

Table 1 The environmental covariates used in this study.

Covariates	Code	Description	Unit
Edaphic variables	CFRAG	Coarse fragments (>2mm)	%
	BULK	Bulk density	g cm^{-3}
	ORGC	Organic carbon	g kg^{-1}
	SDTO	Sand content	%
	CLPC	Clay content	%
	STPC	Silt content	%
	TAWC	Available water capacity	cm m^{-1}
	TOTN	Total nitrogen	g kg^{-1}
	CNrt	C:N ratio	-
	PHAQ	pH measured in H_2O	-
Climatic variables	T1	Annual mean temperature	°C
	T2	Mean diurnal range	°C
	T3	Isothermality (T2/T7×100)	%
	T4	Temperature seasonality (standard deviation×100)	°C
	T5	Max temperature of warmest month	°C
	T6	Min temperature of coldest month	°C
	T7	Temperature annual range (T5–T6)	°C
	T8	Mean temperature of wettest quarter	°C
	T9	Mean temperature of direst quarter	°C
	T10	Mean temperature of warmest quarter	°C
	T11	Mean temperature of coldest quarter	°C
	P1	Annual precipitation	mm
	P2	Precipitation of wettest month	mm
	P3	Precipitation of driest month	mm
	P4	Precipitation seasonality (coefficient of variation)	%
	P5	Precipitation of wettest quarter	mm
	P6	Precipitation of driest quarter	mm
	P7	Precipitation of warmest quarter	mm
	P8	Precipitation of coldest quarter	mm
	MATG	Mean annual temperature during growing season	°C
	MATNG	Mean annual temperature during non-growing season	°C
	MAPG	Mean annual precipitation during growing season	mm
	MAPNG	Mean annual precipitation during non-growing season	mm
Grassland type	-	Meadow, typical and desert steppe	-
Livestock	-	Cattle, sheep and goat	head km^{-2}

Table 2 Summary of Inner Mongolian grassland aboveground (AGB) biomass during different periods

CO_2 enrichment effects	Climate change scenario	Period	AGB across grassland types (kg ha^{-1}, mean±SD)			
			Meadow	Typical	Desert	All
Not included	RCP4.5	2020−2039	1,934±112	1,345±201	918±287	1,304±181
		2040−2059	1,837±171	1,223±235	768±340	1,174±249
		2060−2079	1,916±117	1,312±184	779±275	1,253±191
		2080−2100	1,965±97	1,306±170	702±279	1,237±181
	RCP8.5	2020−2039	1,902±107	1,269±156	740±294	1,206±163
		2040−2059	1,862±142	1,230±245	733±304	1,165±252
		2060−2079	1,800±123	1,219±193	722±308	1,169±202
		2080−2100	1,672±140	1,087±156	666±236	1,033±162
Included	RCP4.5	2020−2039	2,187±161	1,597±224	1,171±340	1,557±220
		2040−2059	2,520±199	1,906±264	1,451±346	1,857±272
		2060−2079	2,919±143	2,315±217	1,782±295	2,256±223
		2080−2100	3,067±103	2,408±172	1,804±283	2,339±184
	RCP8.5	2020−2039	2,274±166	1,642±176	1,113±307	1,579±177
		2040−2059	3,012±261	2,380±314	1,882±345	2,315±310
		2060−2079	4,097±331	3,517±351	3,018±471	3,466±360
		2080−2100	5,423±470	4,838±503	4,417±585	4,784±512

455

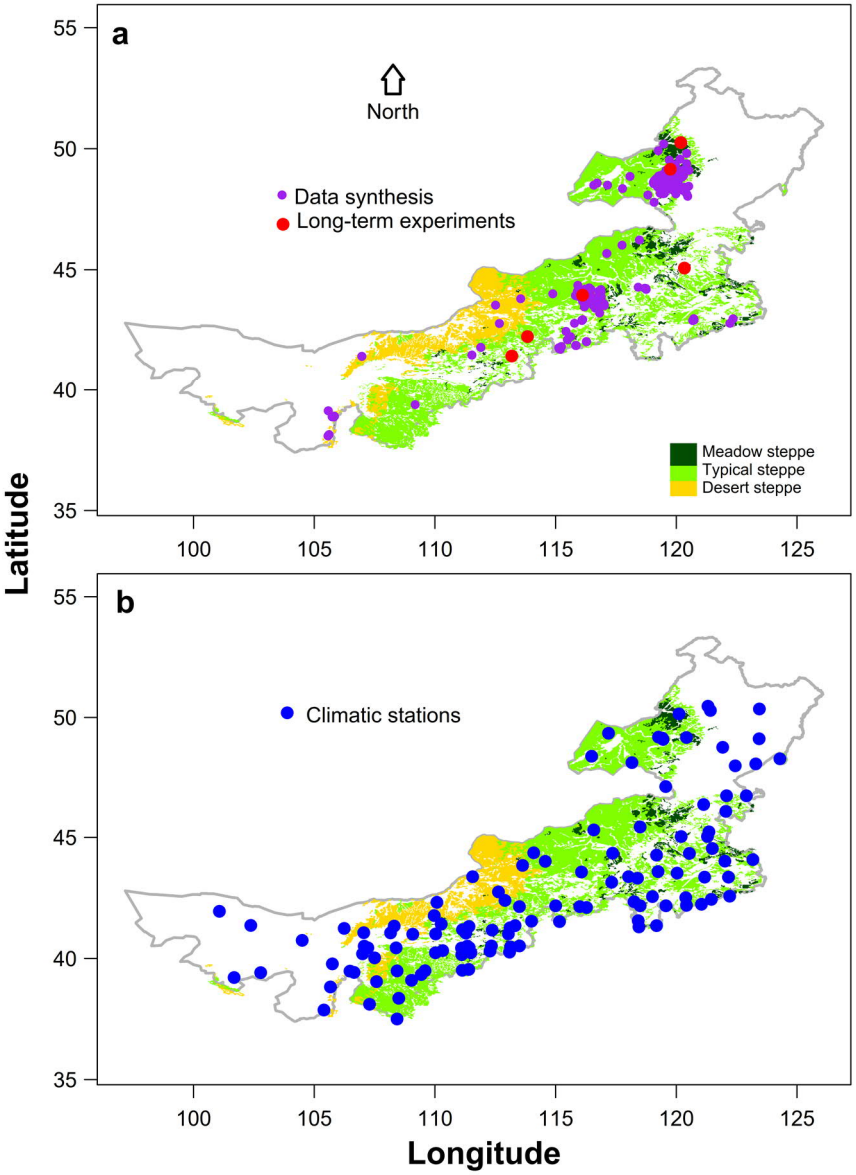

Figure 1. Spatial distribution of grassland aboveground biomass observations (a) and the 120 climatic stations (b) in Inner Mongolia. The Inner Mongolian grasslands are grouped into three categories (i.e., meadow steppe, typical steppe and desert steppe). Observations of grassland biomass are both derived from literature synthesis and the six long-term experimental sites. The ground climatic records are obtained from China's national meteorological bureau.

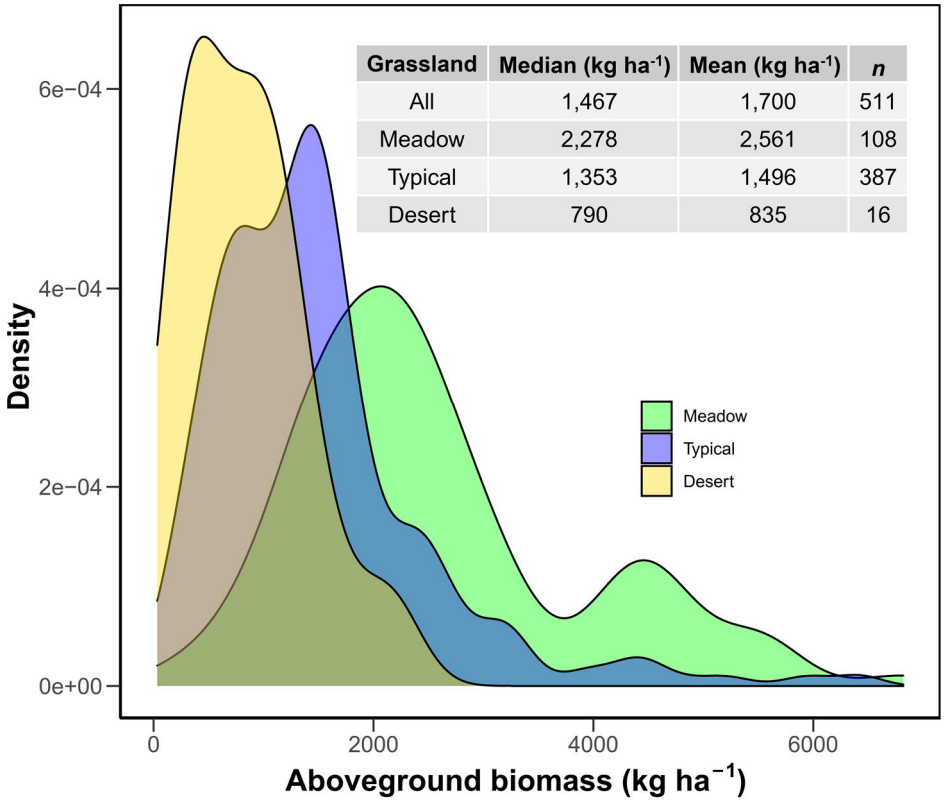

Figure 2. Aboveground biomass distribution across different grassland types in Inner Mongolia. See Fig. 1 for the spatial distribution of the three grassland types in Inner Mongolia.

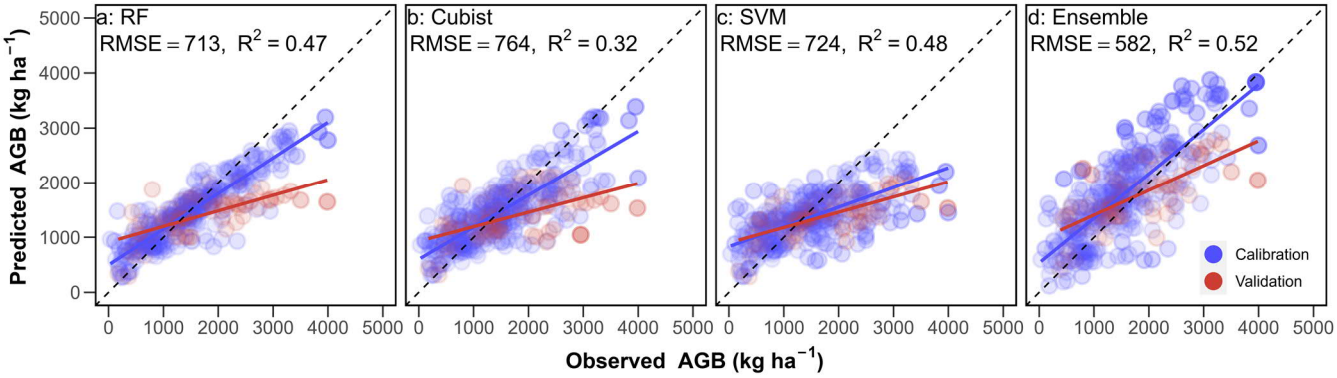

Figure 3. Performance of fitted machine learning-based models to predict grassland aboveground biomass (AGB). a, random forest (RF); b, Cubist; c, support vector machines (SVM); d, the ensemble model of a-c. For each individual model, 80% of the stratified samples of observations were used for model calibration, with the other 20% used for validation. R^2 and RMSE show the coefficient of determination and root mean square error of model validations. In model calibrations, the R^2 is 0.82, 0.66 and 0.43 for RF, Cubist and SVM, respectively, and RMSE is 359 kg ha^{-1}, 460 kg ha^{-1} and 579 kg ha^{-1}, respectively for RF, Cubist and SVM, respectively.

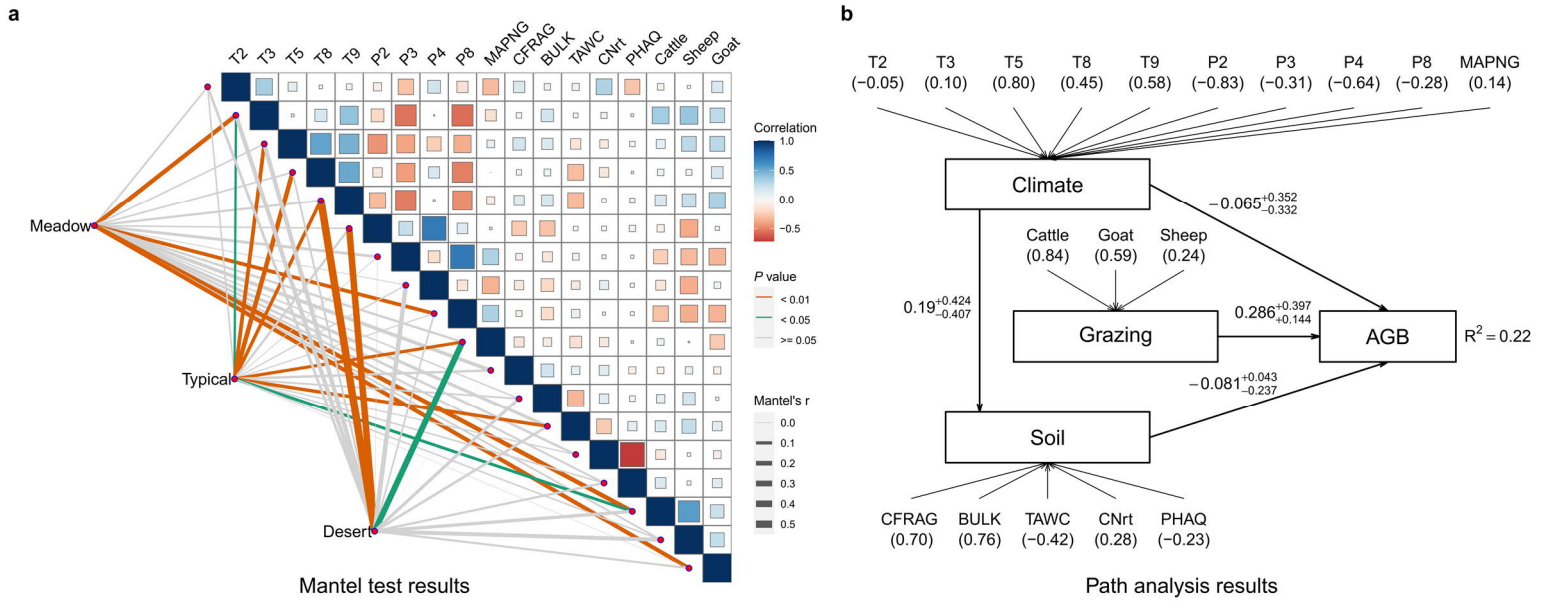

Figure 4. Environmental drivers of Inner Mongolian grassland biomass. a, the correlation matrix of environmental drivers and mantel test results. The upper triangle shows the pairwise comparisons of predicting variables, with a color gradient denoting Spearman's correlation coefficient. Taxonomic grassland type (i.e., meadow, typical and desert steppe) was related to each environmental factor by partial (geographic distance–corrected) Mantel test. Line color represents the statistical significance and line width denotes the Mantel's r statistic for the corresponding distance correlations. b, the path analysis results of the direction and magnitude of the effects of latent variable climate (reflected by T2, T3, T5, T8, T9, P2, P3, P4, P8 and MAPNG indicated by function *findCorrelation* in R package *caret* to exclude the environmental covariates with high multicollinearities, hereafter the same for soil), soil (using CFRAG, BULK TAWC, CNrt and PHAQ as indicators) and grazing (using Cattle, Goat and Sheep as indicators) on AGB (grassland aboveground biomass). Numbers in parentheses represent the loadings (correlation coefficients) of the indicators to the latent variables. See Table 1 for descriptions of each variables and see details in Materials and Methods section for the statistical analysis.

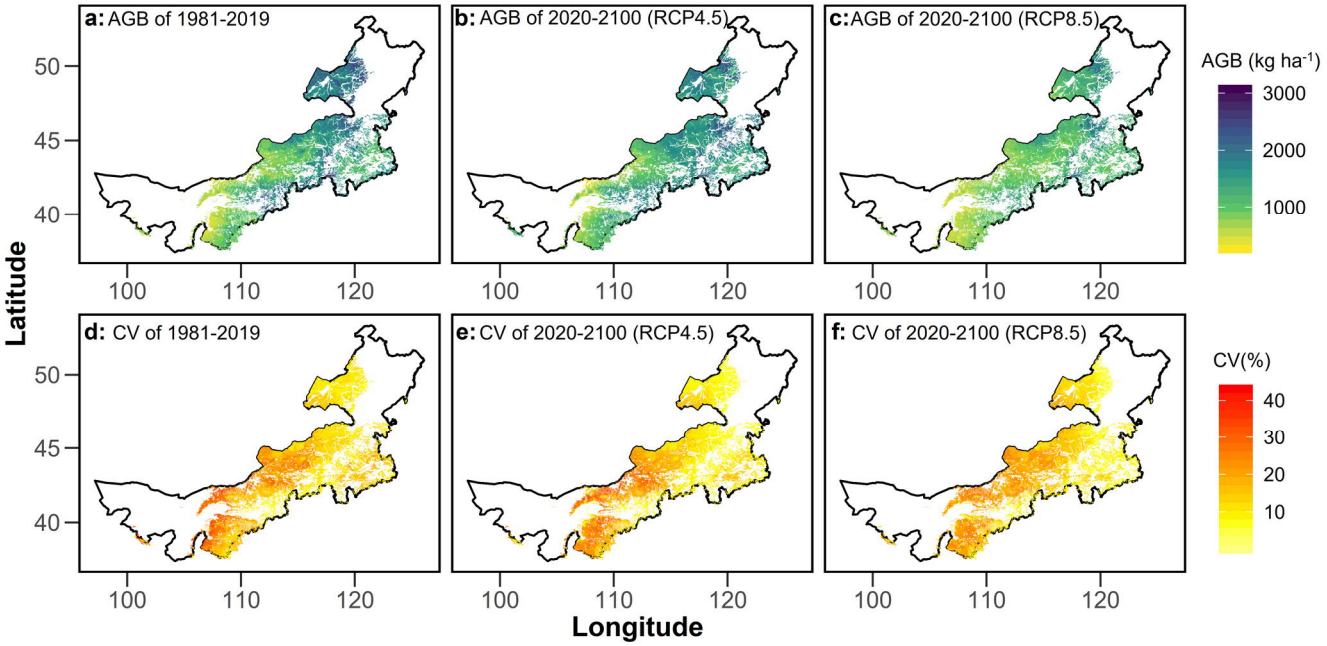

485

Figure 5. Spatial patterns of Inner Mongolian grassland aboveground biomass (AGB) and the uncertainties in terms of coefficient of variations (CV). The upper panel shows the average gridded AGB over 1981-2019 (a) and under two climate change scenarios [RCP4.5 (b) and RCP8.5 (c)] over 2020-2100. The lower panel (d, e and f) exhibit the associated CV of the upper panel. These estimations are derived from simulations without considering the CO_2 enrichment effects on AGB.

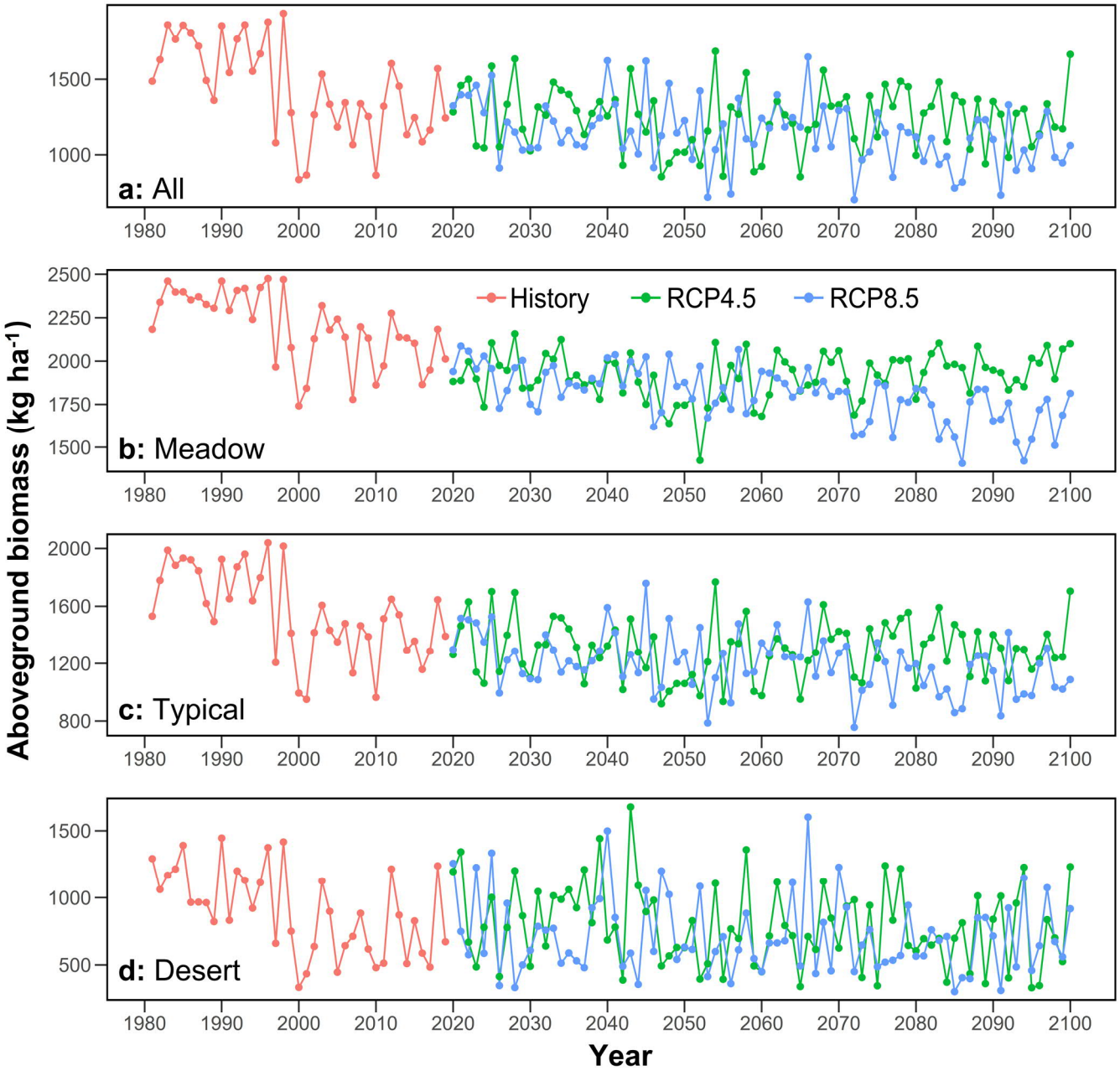

490

Figure 6. Temporal variations of the predicted average aboveground biomass (AGB) in Inner Mongolian grasslands. At each year, data are averages of all the 1km×1km grids (a) and across a certain grassland type at the regional scale (b, c and d), these estimations are derived from simulations without considering the CO_2 effects on AGB.

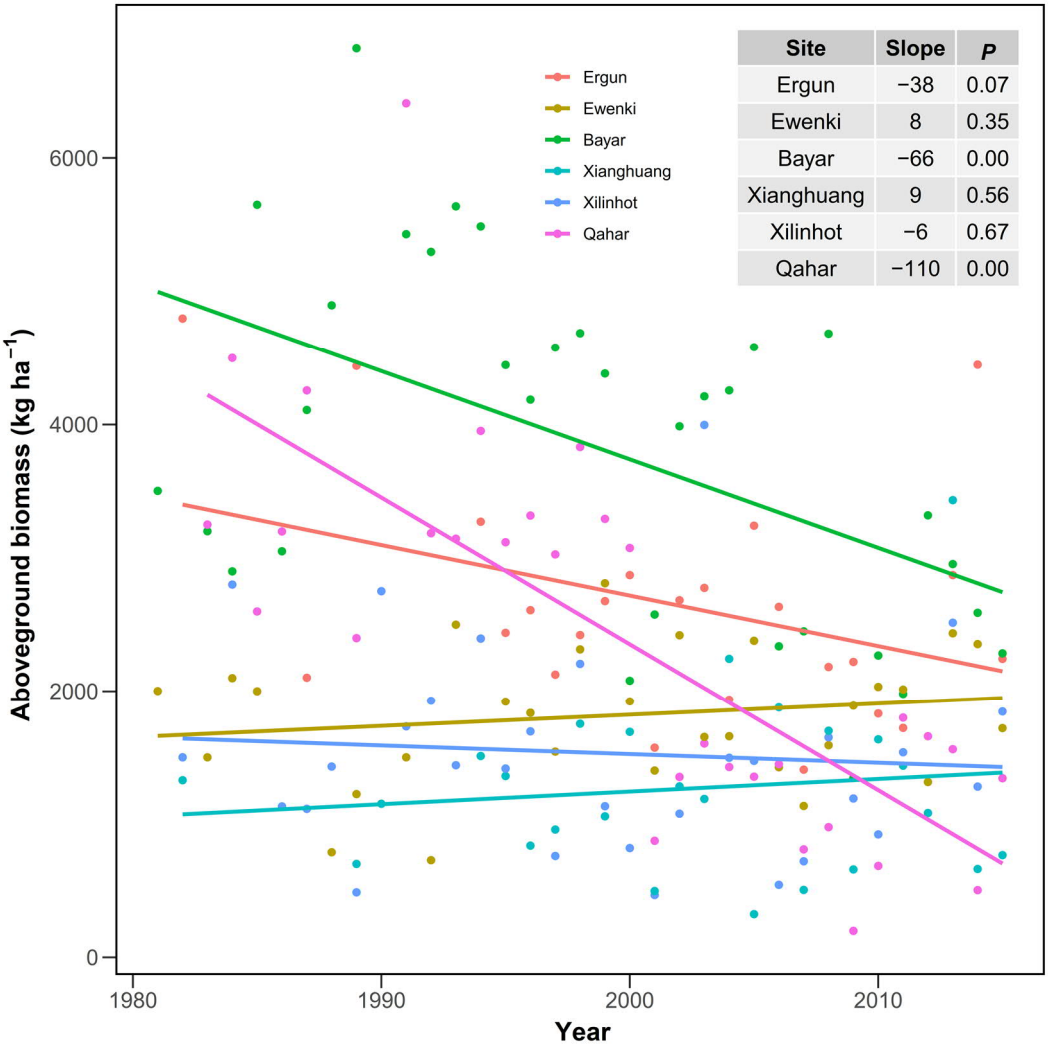

495 **Figure 7. Temporal changes in aboveground biomass (AGB) in the six long-term filed experiments in Inner Mongolian grassland.** Table shows the linear trends (slope, kg ha^{-1} yr^{-1}) and significance (*P* value) of the variations in AGB.

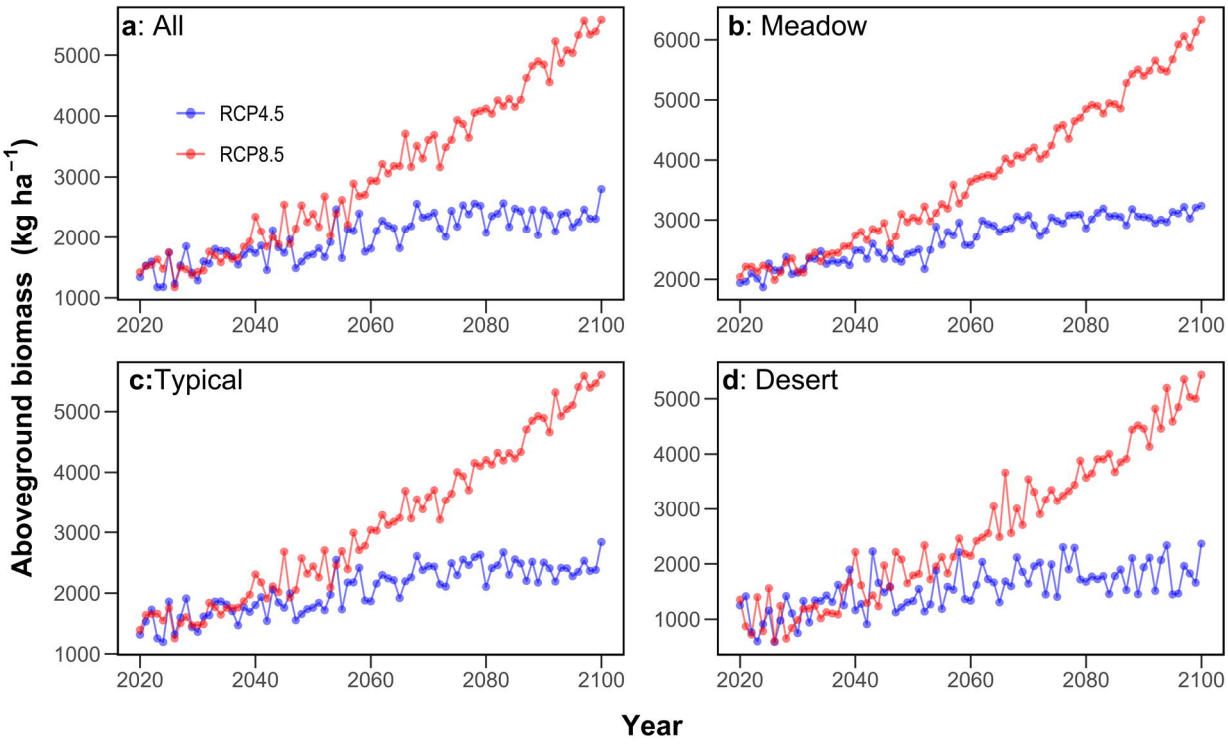

Figure 8. Temporal variations of the projected future aboveground biomass (AGB) in Inner Mongolian grasslands. a-d: temporal changes in AGB of all grasslands, meadow, typical and desert steppe, respectively. In these estimations, the effects of CO_2 enrichment on AGB are included.